NMR propagator measurements on flow through a random pack of porous glass beads and how they are affected by dispersion, relaxation, and internal field inhomogeneities

U. M. Scheven*
Schlumberger-Doll Research, 36 Old Quarry Road, Ridgefield, Connecticut 06877, USA

J. G. Seland and D. G. Cory
Department of Nuclear Engineering, Massachusetts Institute of Technology, Cambridge, Massachusetts 02139, USA
(Received 2 September 2003; revised manuscript received 27 October 2003; published 20 February 2004)

We flow water through a pack of porous glass beads and employ NMR to measure molecular displacement distributions—the propagators—in the Stokes flow regime. Fluid is flowed over several evolution times to attain fixed mean displacements, and the time dependence of the resulting propagators is analyzed for the effects of diffusion, NMR relaxation, and signal loss due to internal fields. We delineate and illustrate the experimental regimes in which these different effects make their presence felt. Simulations on a simple model system reproduce the essential features of our experimental results and provide insight into the mechanisms shaping the propagators.

DOI: 10.1103/PhysRevE.69.021201 PACS number(s): 47.55.Mh

I. INTRODUCTION

Tracer dispersion and fluid flow in porous media are of great practical importance in biological perfusion, the cleanup of contaminated soils, the design of chemical reactors and catalytic particles, and in oil recovery. It is also of significant theoretical interest, due to the complicated interplay of mechanical and diffusive mixing processes [1–5]. Experimentally, molecular motions and dispersion in porous media have been investigated for some time with various nuclear magnetic resonance (NMR) techniques, for example, measurements of free molecular diffusion [6], restricted diffusion [7], or measurements of propagators [8], the probability distribution of diffusive and advective molecular displacements. These have been studied intensively for different types of porous media [9–17], for example, in random packs of monodisperse spheres, artificial porous media, and rocks. NMR experiments on fluid in rocks present particular challenges. Carbonate rocks, which contain much of the world's oil reserves, are characterized by complex pore spaces arising from varied growth or depositional environments, for example in coral reefs or in deposits of dead marine organisms, and shaped by subsequent morphology changing processes, for example erosion, dissolution, and reprecipitation. The length scales of the pore space in a carbonate rock can range from submicrometers to centimeters in the same sample. Sandstones, on the other hand, tend to have less complex pore spaces, but macroscopic layering and magnetic impurities and clays are often present, all of which can have profound effects on NMR measurements of dispersion. In this paper we report on propagator measurements of water flowing through a pack of microporous, near monodisperse glass beads. Our experiments approximate the dispersion and NMR phenomena occurring in natural porous media, in several important ways. First, the presence of two length scales—the bead diameter d and the length scale l of the pores inside the beads ($l \ll d$)—gives rise to a heterogeneous flow field with significant stagnant zones known to be quite important in dispersion phenomena [5,18]. Second, enhanced surface relaxation of the NMR signal from fluid near pore walls skews propagator measurements or measurements of dispersion coefficients. This effect is present in the measurement whenever the relaxation rates for fluid contained in the porous medium are faster the bulk relaxation rates. Finally, inhomogeneous internal magnetic fields in the sample distort the propagators measured with pulsed field gradient (PFG) NMR [19]. This effect is present in the measurement whenever there is a susceptibility difference between the fluid and the matrix. Here we keep track of all these effects, and in the process describe the experimental parameters and a general conceptual framework suitable for the study of preasymptotic flow and NMR effects in naturally occurring porous media. Our quantitative results are sufficiently accurate to permit self-consistency checks and a quantitative analysis, as well as a comparison with an instructive and reductive model of flow in the presence of hold-up and surface relaxation.

Section II gives some elementary background about asymptotic and preasymptotic dispersion, and how that affects the design of our experiment. Section III describes particulars of sample preparation and NMR measurements followed by Sec. IV with a discussion of results. The simulations are described in Sec. V, followed by conclusions in Sec. VI.

II. MOTIVATION

Mixing in flow through porous media occurs through the interplay of two processes, diffusion and mechanical mixing. The asymptotic behavior of either process can be understood in terms of Einstein's argument. A diffusive random walk with step length l and characteristic frequency τ^{-1} gives rise to an asymptotic ($t \gg \tau$) Gaussian displacement distribution with $\sigma = \sqrt{2D_m t}$. The molecular diffusion coefficient is $D_m = l^2/\tau$. For mechanical mixing, members of an ensemble of

*Electronic address: scheven@slb.com

fluid elements are advected by a mean displacement $\langle\zeta\rangle$ in a porous medium of characteristic pore size d, executing a random walk with spatial frequency d^{-1}. Upon collision with an obstacle the fluid elements are scattered with step length $l_m=\beta d$, $\beta<1$, giving rise to an asymptotic ($\langle\zeta\rangle\gg d$) Gaussian distribution of displacements about the mean with $\sigma=\sqrt{2D'\langle\zeta\rangle}$. The dispersivity is $D'=\beta^2 d$, and β is a scattering parameter characteristic of the sample. Asymptotic dispersion for the case where diffusion and mechanical mixing are not separable was first studied by Taylor [1,2] and Saffman [3,4]. Generally, the asymptotic behavior will depend on the Péclet number $\mathrm{Pe}=vd/D_m=t_D/t_v$, which combines the space and time dependence of the mixing process in the ratio of the times required to diffuse or advect a characteristic length d, where v is the fluid velocity. For there to be asymptotic dispersion in a flow experiment, each fluid element or tracer has to have sampled a flow environment representative of the entire pore space, and it must have done so often enough to be in the large-N limit of the random walk executed in the pore space. In contrast to the asymptotic case outlined thus far, preasymptotic dispersion will not depend on time t or distance $\langle\zeta\rangle$ or Péclet number Pe alone, but on some or all of them.

In this paper we focus on the preasymptotic regime, where experimental evolution times Δ were short compared to the time required to diffuse one bead diameter, and mean fluid displacements ranged up to no more than a few bead diameters. We therefore study preasymptotic dispersion [17] with NMR measurements of propagators as a function of displacement and time independently, rather than as a function of P_e. This approach not only is appropriate to the early mixing processes, but also yields quantitative measurements of the NMR effects of surface relaxation and internal field inhomogeneities which might otherwise be attributed to the mixing process. One may think, for example, of stagnation peaks in propagators, which can vanish by some combination of dispersion and diffusion or by NMR relaxation alone, as experimental evolution times get longer. Measurement of the NMR effects described in this work thus serves as a check on the simultaneous quantitative PFG NMR measurements of dispersion, and is applicable to any quantitative measurement of stagnant zones, or of permeability heterogeneities in the flow field of nonideal samples, such as carbonate or sandstone rocks. Our measurements also permit quantitative comparisons of propagator data with simulations incorporating surface relaxation, as surface relaxation produces measurable displacement-relaxation correlations in the preasymptotic regime.

III. EXPERIMENTS

A random pack of water-wet microporous glass beads [20] with a bead diameter of 150 ± 25 μm and submicrometer (3000 Å) pore scale of the beads' porosity was placed in a glass NMR tube with an inner diameter of 8 mm. The total porosity of the sample was $\phi=0.66\pm0.03$, roughly half of which is attributable to micropores. Water was flowed through the pack for fixed mean displacements denoted by $\langle\zeta\rangle_0=\Delta\dot{V}/A\phi$, where Δ is the evolution time, $\dot{V}$ is the volumetric flow, A is the cross section of the sample, and ϕ is its porosity. Constant flow was established with an ISCO-1000D piston pump, and all flow reported here was in the Stokes flow regime with Reynolds number ($\mathrm{Re}<1$). Several fixed $\langle\zeta\rangle_0$ between 125 and 600 μm were attained over seven suitably chosen evolution times Δ between 30 and 600 ms, with mean drift velocities adjusted to $\langle v\rangle=\langle\zeta\rangle_0/\Delta$. The idea behind the experimental procedure is straightforward. In the absence of diffusion, relaxation, or experimental artifacts, the measured propagators for a given $\langle\zeta\rangle_0$ should be independent of the time Δ taken to produce it, because the Stokes flow field and the geometry imposing it are time independent. The actually measured shape and time dependence of these propagators can therefore be used in a quantitative analysis of the pore space in terms of diffusive coupling between stagnant and moving fluid, and in terms of NMR relaxation, signal suppression by flow through inhomogeneous background fields, or nonlinear flow phenomena if they were present.

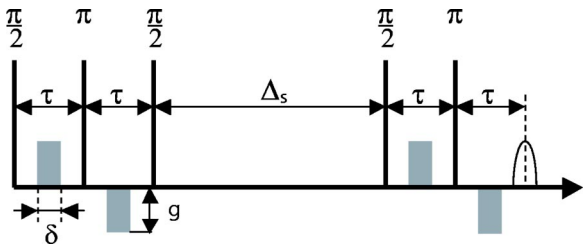

FIG. 1. APGSTE pulse sequence, with gradient pulses shown in gray and rf pulses as solid lines. The stimulated echo amplitude at $t=4\tau+\Delta$ is proportional to the ensemble average $\langle e^{iq\zeta}\rangle$ of the phase factors associated with the displacements of protons during the experimental evolution time $\Delta=\Delta_s+3\tau/2-\delta/6$.

The propagators for each choice of $(\langle\zeta\rangle_0,\Delta)$ were produced from PFG NMR measurements made in the 3 T field of a horizontal bore superconducting magnet, using a Bruker AMX NMR console. We employed the standard 13-interval alternating pulsed gradient stimulated echo [21] (APGSTE) sequence commonly employed for such experiments, shown in Fig. 1. Separated by a storage interval Δ_s, there are spatial coding intervals of duration 2τ during which the magnetization is sensitive to applied field gradients, shown in gray in Fig. 1, which encode or decode the position of proton spins in the phase of their magnetization. During the coding intervals the magnetization is also sensitive to background fields produced by susceptibility differences between the fluid and the matrix. We note for future reference that the refocusing π pulses at the center of the spatial coding intervals serve to eliminate unwanted precession produced by susceptibility induced internal field offsets, for spins experiencing the same time averaged internal offset fields during the intervals τ before and after the pulse.

The NMR signal at $t=4\tau+\Delta_s$ is proportional to the ensemble average of phase factors $\langle e^{i\theta}\rangle$ over all polarized spins, where $\langle e^{i\theta}\rangle=\int P'(\theta',\Delta)e^{i\theta'}d\theta'$ defines the normalized probability distribution $P'(\theta,\Delta)$ of phase factors $e^{i\theta}$ after an evolution time Δ. Neglecting NMR relaxation and dephasing effects, which are the subject of this paper and will be discussed at length further on, the APGSTE pulse

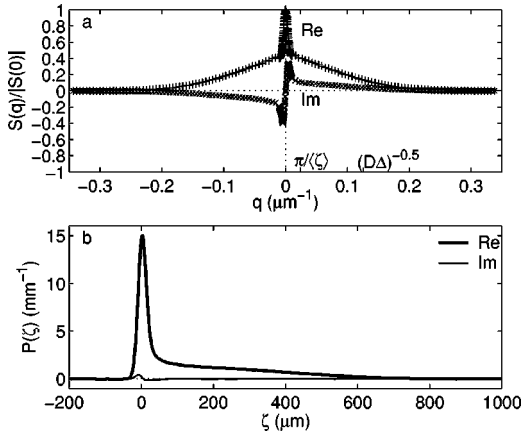

FIG. 2. (a) Real and imaginary PFG NMR signal $S(q)/|S(0)|$ as a function of $q=\gamma(2\delta)g_z$ for flow through a porous bead pack with $\Delta=30$ ms and $\langle\zeta\rangle_0=132$ μm. (b) Propagator derived by Fourier transforming the data shown in (a).

sequence produces a phase shift $\theta=\zeta q$ in the magnetization of each spin displaced by a distance ζ during the evolution time $\Delta=\Delta_s+\frac{3}{2}\tau-\frac{1}{6}\delta$, where $q=\gamma(2\delta)g_z$ is the wave vector set up by the pulsed field gradients. Δ_s, τ, and δ are the storage time, the echo time, and the duration of a single gradient pulse, respectively, $\gamma=2\pi\times4257$ Hz/G is the gyromagnetic ratio of protons, and g_z is the amplitude of the pulsed field gradient. With a linear relationship between phase and displacement, the NMR signal can be rewritten as $\langle e^{iq\zeta}\rangle=\int P(\zeta',\Delta)e^{iq\zeta'}d\zeta'$, where the earlier probability distribution of phases $P'(\theta,\Delta)$ has now been replaced by a probability distribution of displacements, the propagator $P(\zeta,\Delta)$. The NMR signal is the qth Fourier component of this propagator, which we measure for suitably chosen values of q for all flow speeds and times. From these measurements we obtain the probability distributions $P(\zeta,\Delta)$ by Fourier transform, which we shall refer to as propagators even when the linear relationship between phase and displacement is distorted by relaxation and dephasing effects. We employed gradients of duration 4 ms and maximal gradient strength of 25 G/cm, and echo times $\tau=5$ ms. The active length L of the NMR coil was $L\approx19$ mm.

IV. RESULTS

A. Optimized acquisition

We first consider in detail the PFG NMR data set $S(q)$ and the propagator derived from it shown in Fig. 2, in order to illustrate the nature of the flow field and our experimental procedure. The NMR signal is measured up to $|q|\simeq0.35$ μm^{-1}, in an experiment with $\langle\zeta\rangle_0=132$ μm and an experimental time $\Delta=30$ ms much shorter than the time $t_D=r^2/D_m\simeq2.7$ s needed by a molecule to diffuse one sphere radius $r=75$ μm. Hence the NMR signal arises from the sum of two nearly unmixed components of the fluid $S(q)=f\langle e^{iq\zeta}\rangle_a+(1-f)\langle e^{iq\zeta}\rangle_D$, where the predominantly advective first term is associated with the fraction f of the fluid carried along by the Poiseuille flow field between spheres, while the diffusive second term is associated with the stagnant fraction of the fluid located within the microporous spheres. The advective and diffusive terms are identified readily in the data shown in Fig. 2(a), because of their very different dependence on q. Advection shifts and then scrambles the phases of molecules carried along by the Poiseuille flow field, over a small range of $|q|<f2\pi\langle\zeta\rangle^{-1}\simeq\pi\langle\zeta\rangle^{-1}$, indicated in Fig. 2(a). The real part of the signal drops by about 55% with considerable signal appearing in the imaginary part. As $|q|$ gets larger the advective term $f\langle e^{iq\zeta}\rangle_a$ goes to zero, and only the diffusive term $(1-f)\times\langle e^{iq\zeta}\rangle_D$ remains. This term tends to zero as $|q|$ becomes much larger than the inverse diffusion length $1/\sqrt{D\Delta}$, also indicated in Fig. 2(a). These observations illustrate how the inverse mean displacement and the inverse diffusion length of an experiment set the scales for an efficient sampling of $S(q)$, which we perform with 128 equally spaced measurements covering a small range of q around $q=0$ up to $|q|\simeq f2\pi/\langle\zeta\rangle$, and with a second set of 128 q values covering q space more coarsely up to $|q|\gg1/\sqrt{D\Delta}$. The two data sets are combined, regridded by linear interpolation, and zero filled for improved signal to noise ratio and resolution. Upon fast Fourier transform one obtains the real propagator $P(\zeta)$ shown in Fig. 2(b). The data shown in Fig. 2(a) already exhibit, to the eye, the symmetry $S(-q)=S^*(q)$ required for an underlying real probability distribution. The symmetry is confirmed by the fact that the imaginary part of the propagator, shown in Fig. 2(b), is essentially zero except for some small residual signal near $\zeta=0$ arising from experimental artifacts. All our propagators cover displacements up to several millimeters, with a resolution of a few micrometers. It is worth pointing out that the quality of our NMR derived propagators is made possible by our *a priori* knowledge of mean displacement, experimental time scale, and diffusion coefficient, permitting a more efficient sampling of q space, compared to the sampling with equal q spacings commonly employed in NMR propagator experiments.

B. Surface relaxation and susceptibility

We now illustrate the presence and relevance of three mechanisms which can shift the spectral weight of propagators, such as the one shown in Fig. 2(b), depending on the length of time Δ taken to attain a given mean displacement $\langle\zeta\rangle_0$. First, diffusion of molecules across streamlines and between stagnant and flowing parts of the flow field will couple slow and fast parts of the flow field, shifting spectral weight from the undisplaced and the most displaced parts of the spectrum toward its mean. Evidence for both will be given further below. Second, spectral weight is shifted because enhanced surface relaxation preferentially removes the signal of spins in small pores, where molecules collide with relaxing pore walls at a higher frequency than in large pores. The inhomogeneous surface relaxation produces an undercount of stagnant spins in the small pores, and a corresponding overcount of the flowing spins in large pores. Surface relaxation is evident in the inversion recovery measurements shown in Fig. 3(a), where the mean measured relaxation time of $\langle T_1\rangle=790$ ms is reduced from the bulk value of the fluid $T_{1b}\simeq3$ s. For consistency the velocity independence of sur-

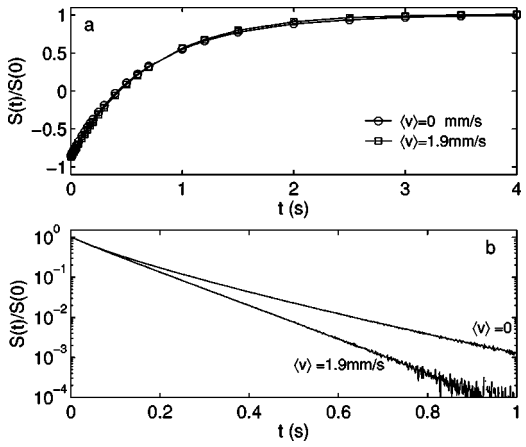

FIG. 3. (a) Inversion recovery measurement of T_1 relaxation. Surface relaxation depresses $\langle T_1 \rangle \simeq 790$ ms below the bulk value for water ($T_{1b} \simeq 3$ s). (b) The CPMG measurement of T_2 relaxation with echo spacing $2\tau_e = 1.6$ ms. The measurement is sensitive to surface relaxation *and* to molecular displacements. Displacements by Brownian motion through spatially varying internal fields attenuate the signal ($T_2 = 100$ ms$\ll T_1$). Superimposed flow produces larger displacements and attenuates the signal further.

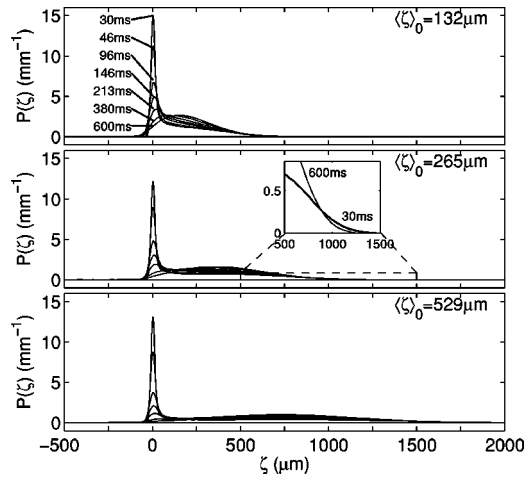

FIG. 4. Propagators obtained for mean displacements $\langle \zeta \rangle$ between 132 and 529 μm, with the same flow times Δ between 30 and 600 ms for all three mean displacements. The inset shows evidence for diffusion across streamlines, whereby the large displacement tail at $\Delta = 30$ ms has disappeared by the time $\Delta = 600$ ms.

face relaxation was verified with measurements in the presence and absence of flow. Third, spectral weight is shifted because the flow displaces spins through the spatially varying internal fields of the pore space during spatial coding intervals. This displacement may suppress the signal from spins residing on the fastest streamlines, because these fast spins may not experience the same time averaged internal offset fields before and after the refocusing π pulse at the center of the spatial coding intervals. In the presence of significant background fields ($\overline{\delta B}\gamma\tau \gtrsim 1$), this suppression is expected to arise, at least, for spins advected by the pore length d during spatial coding, due to the randomness of the pore space. Internal field inhomogeneities and the signal attenuation they produce are confirmed with CPMG T_2 relaxation measurements shown in Fig. 3(b). These were conducted with and without flow, with $\tau_e = 0.8$ ms. In the absence of flow the measured $T_2 \ll T_1$ because the signal of spins diffusing about in the inhomogeneous internal fields of the rock is refocused poorly. The offset fields are therefore non-negligible, and they do produce signal suppression. When flow is present, refocusing of the magnetization is worse still, and the signal is suppressed further, as spins are advected through the internal offset fields, which vary at the pore scale [22]. We shall see below that in our propagator measurements the combined effects of flow induced displacement and internal fields also become apparent, for experiments where spins are displaced by more than a pore length during our spatial coding intervals of duration 2τ.

C. Quantitative propagators

Three sets of propagators obtained for mean displacements $\langle \zeta \rangle_0$ of 132, 265, and 529 μm are shown in Fig. 4. The flow times Δ were the same for all three sets of experiments and ranged from 30 to 600 ms, corresponding to free diffusion lengths $l_D = \sqrt{D\Delta}$ from 8 to 35 μm. Experimental diffusion lengths thus range from a small to an appreciable fraction of a bead radius, determining the degree of diffusive coupling between the fluid contained within the porous beads and in between them. For all three mean displacements $\langle \zeta \rangle_0$ propagators obtained with the shortest evolution time ($\Delta = 30$ ms) show a large peak centered around zero displacement, a signature of the stagnant fluid contained within the porous beads. The width and also height of the stagnation peaks, when measured with respect to the background signal provided by the long time ($\Delta = 600$ ms) propagator, are comparable for the three mean displacements. The remainder of the propagators' spectral weight is found in a broad, asymmetric, and rounded ''bump'' at larger displacements, a signature of the flowing fluid between the spheres. Unsurprisingly, it is more stretched out for propagators with larger mean displacements. With longer Δ the area under the stagnation peaks decreases and spectral weight shifts toward larger displacements. Additionally, some spectral weight, which at short times appeared at the largest displacements, has, at later times, shifted toward the mean displacements.

We analyze the propagators for the effects of the three mechanisms affecting their shapes, namely, diffusion, relaxation, and velocity attenuation of the signal. These are distinguished by their effects on the measured mean displacement $\langle \zeta \rangle_m$, which is to be compared with the actual mean displacement $\langle \zeta \rangle_0$ set by sample size, porosity, flow rate, and flow time Δ. Diffusive exchange preserves $\langle \zeta \rangle_m = \langle \zeta \rangle_0$, unequal surface relaxation can produce an undercount of stagnant fluid in micropores, with $\langle \zeta \rangle_m > \langle \zeta \rangle_0$, and flow displacement in inhomogeneous internal fields can produce an undercount of spins in the streamlines with fastest flow, with $\langle \zeta \rangle_m < \langle \zeta \rangle_0$. The mean measured displacement $\langle \zeta \rangle_m$ is determined in two ways, shown in Fig. 5 for the data set with $\Delta = 30$ ms and $\langle \zeta \rangle_0 = 265$ μm. First, the phase of the NMR signal for small $|q|$ is fitted to a linear plus a cubic term, corresponding to the first and third terms of the cumulant [23] expansion of the NMR signal $\ln_{10}\langle e^{iq\zeta} \rangle$

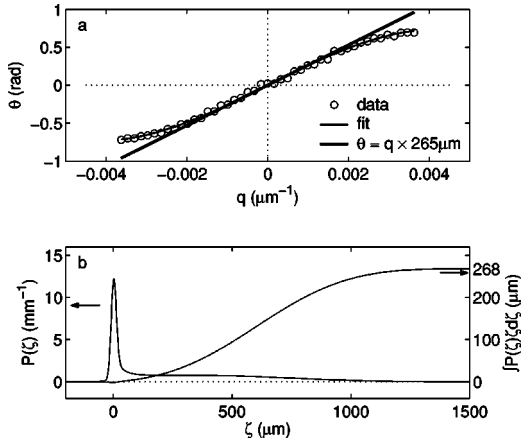

FIG. 5. Two ways of measuring the mean displacement $\langle\zeta\rangle_m$ for $\Delta=30$ ms and $\langle\zeta\rangle_0=265$ μm. (a) The phase of the NMR signal vs q. The slope of the linear term, shown as a solid line, measures a mean displacement of $\langle\zeta\rangle_m=265$ μm. (b) The numerical integration of $\int P(\zeta)\zeta d\zeta$ measures the mean displacement of $\langle\zeta\rangle_m=268$ μm.

$=\Sigma_{j=1}^{\infty}[(iq)^j/j!]X_j$, with $X_1=\langle\zeta\rangle_m$. Second, the mean displacement is measured by integration of $\langle\zeta\rangle_m=\int P(\zeta)\zeta d\zeta$. Both methods of measuring $\langle\zeta\rangle_m$ were applied to all propagators, and the data are compiled in Fig. 6. The results obtained by fitting the phase and by integration agree very well for the experiments with nominal mean displacements $\langle\zeta\rangle_0$ of 132 and 265 μm, and to within $\approx$12% for those with a $\langle\zeta\rangle_0$ of 529 μm. The curves for a $\langle\zeta\rangle_0$ of 132 and 265 μm are similar. For the shortest time $\Delta=30$ ms the measured mean displacements coincide with their respective $\langle\zeta\rangle_0$. As Δ grows, surface relaxation increasingly removes slow or stagnant spins from the measurement, raising $\langle\zeta\rangle_m$ by 50% above $\langle\zeta\rangle_0$ as Δ grows to 600 ms. The results for propagators with a $\langle\zeta\rangle_0$ of 529 μm are somewhat different. While relaxation also enhances measured mean displacements for the

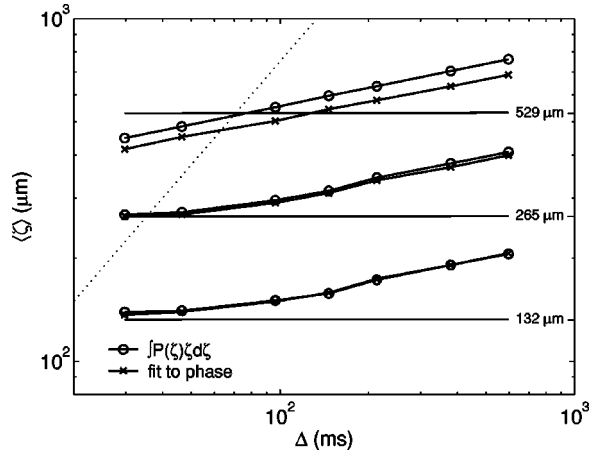

FIG. 6. The measured mean displacement of all propagators, determined by fitting the NMR phase to obtain the first cumulant, and by integrating over the propagator, is plotted against the evolution time Δ taken to attain it. The solid horizontal lines correspond to the experimentally set choices of $\langle\zeta\rangle_0$. Above the dotted line mean flow velocities are larger than $\langle v\rangle=fd/2\tau$.

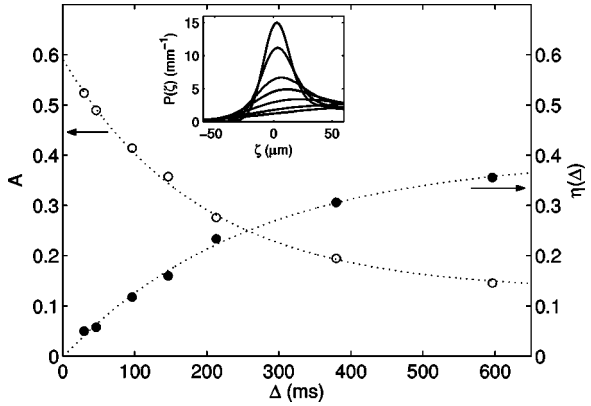

FIG. 7. (●) $\eta(\Delta)=1-\langle\zeta\rangle_0/\langle\zeta\rangle_m$, calculated signal loss by surface relaxation in the stagnation peak, assuming no surface relaxation of advected spins. (○) Measured signal under the stagnation peak, integrated over ±60 μm about the origin. The dotted lines are fits described in the text; the inset shows the stagnation peak over the range of integration.

longer Δ, additional signal is lost from fast streamlines by displacements through nonuniform internal fields. For the largest velocities, i.e., the smallest Δ, the measured mean displacement $\langle\zeta\rangle_m$ is now less than $\langle\zeta\rangle_0$. This effect is important at least for spins advected by a pore length during the spatial coding interval. We plot a dotted line in Fig. 6 corresponding to a velocity $\langle v\rangle=fd/2\tau=\langle\zeta\rangle/\Delta$ given by the fraction $f\approx0.5$ of the pore space where there is flow, the bead diameter d, and the duration of the spatial coding interval. Experiments with flow velocities above this line will displace spins out of a pore during the coding interval, and it is indeed where we observe such velocity induced suppression. We note that in our experiment some spins, preferentially those with large displacements, drift out of the active region of the NMR rf coil during the evolution time Δ. This also suppresses the measured mean displacement. We modeled the drift losses using the measured propagators and the known coil length and found that the suppression of $\langle\zeta\rangle_m$ induced by drift beyond the rf coil is at most 3.5% and therefore negligible.

We now focus our attention on the "slower" propagators with $\langle\zeta\rangle_0=132$ μm and $\langle\zeta\rangle_0=265$ μm, where the shapes of the propagators evolve with Δ by relaxation and diffusion alone. One may ask whether or not the stagnant peaks of Fig. 4 vanish because of relaxation alone, or if diffusion plays a part in their disappearance. In order to answer this question we shall assume for the moment that there is negligible diffusive coupling between flow and stagnation zones, as might actually be the case in a more heterogeneous porous medium. Surface relaxation, which predominantly occurs in the micropores where the surface area is large, would therefore remove a fraction $\eta(\Delta)$ of the overall signal from the signal of the stagnant fluid in the micropores, giving rise to a measured mean displacement of $\langle\zeta\rangle_m=\langle\zeta\rangle_0/[1-\eta(\Delta)]$. Thus $\eta(\Delta)=1-\langle\zeta\rangle_0/\langle\zeta\rangle_m$ measures the presumably relaxed spins, which can then be compared with the measured time dependent area of the stagnation peak. This is shown in Fig. 7 for the propagators with a $\langle\zeta\rangle_0$ of 132 μm. The open

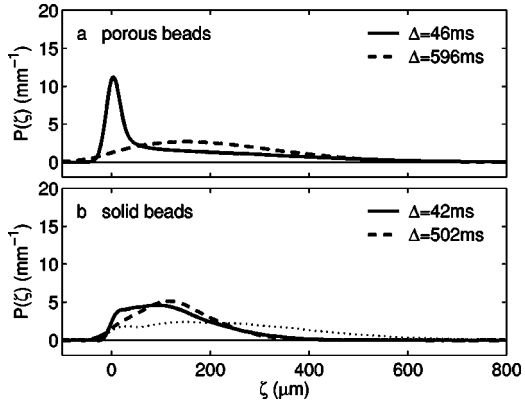

FIG. 8. (a) Propagators of flow through a random pack of porous beads with $d=150\ \mu$m and mean displacement $\langle\zeta\rangle_0=132\ \mu$m. (b) Comparable propagators of flow through a random pack of solid beads with $d=155\ \mu$m and mean displacement $\langle\zeta\rangle_0=128\ \mu$m. The propagator with $\langle\zeta\rangle_0=256\ \mu$m and $\Delta=502$ ms is shown for reference, by the dotted line.

circles denote the area $A(\Delta)$ of the stagnation peak, integrated over the width of the peak from $\zeta=-60\ \mu$m to $\zeta=60\ \mu$m. The inset shows the integrated curves. In order to approximately quantify the magnitude and time dependence of $A(\Delta)$, we have fitted an exponential time dependence plus a constant offset, shown as a dotted line. The fit shows the time dependent spectral weight under the stagnant peak to be $A(\Delta)=0.13+A_0\times e^{-\Delta/\tau_A}$, with $\tau_A=191$ ms and $A_0=0.46$. This is to be compared with the relaxation loss $\eta(\Delta)=(1-\langle\zeta\rangle_0/\langle\zeta\rangle_m)$, shown with filled circles. An exponential fit, again shown as a dotted line through the data, gives $\eta(\Delta)=0.4\times(1-e^{\Delta/\tau_s})$, with $\tau_s=257$ ms. The signal loss from the stagnation zone, as determined by integration, is therefore too large and occurs too rapidly to be attributable to relaxation alone, ruling out our earlier assumption of there being no diffusive coupling between stagnation zones and flowing zones of the flow field at all. Diffusive coupling contributes significantly to the vanishing of the stagnation peaks, with $\delta(\Delta)\equiv A(0)-A(\Delta)>\eta(\Delta)$. The difference $\delta(\Delta)-\eta(\Delta)\simeq 0.08$ for $\Delta=600$ ms represents a lower bound on the fraction of spins which originally resided in stagnant zones, and which have diffused into the flow for the longest time and have been advected beyond our 60 μm limits of integration. Further evidence for the importance of diffusion is provided by an analysis of the T_1 relaxation data shown in Fig. 3(a) in terms of a sum of exponentially decaying components. The analysis shows no significant contribution to the relaxation process at time scales around τ_s or τ_A, which also rules out relaxation as the sole cause for the diminishing stagnation peak.

D. Porous vs nonporous beads

As an experimental consistency check on the picture developed thus far we compare propagators obtained with flow through our pack of porous beads, shown in Fig. 8(a), with those obtained in a separate experiment [17] on water flow through a pack of solid glass beads, shown in Fig. 8(b). The nominal bead sizes for both sets of experiments (d

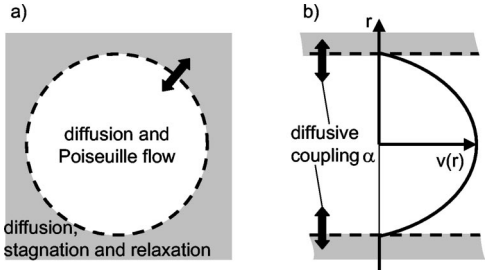

FIG. 9. Schematic diagrams of the modeled pipe with a leaky wall surrounded by stagnating fluid shown in gray, viewed head on (a) and from the side (b). Diffusion and NMR relaxation occur in the gray zones, diffusion and Poiseuille flow in the white zones. α is the probability that a molecule hitting the pipe wall will make it through to the other side. The magnetization in the stagnant zones equilibrates instantaneously.

$\approx 150\ \mu$m) are nearly the same, as are the mean displacements $\langle\zeta\rangle_0\approx 130\ \mu$m and the ranges of evolution times Δ covered. In the porous beads of Fig. 8(a) roughly half the fluid is trapped while the other half carries the flow. It is therefore consistent for the flow portion of those propagators to have an extension and shape comparable to the one obtained in the pack of solid beads with twice the mean displacement ($\langle\zeta\rangle_0=256\ \mu$m), shown in a dotted line in Fig. 8(b). Surface relaxation within the porous beads contributes to the diminution of the stagnation peak and raises the measured mean displacement from $\langle\zeta\rangle_m=140\ \mu$m to $\langle\zeta\rangle_m=205\ \mu$m as Δ is increased from 46 to 596 ms. This is to be compared with the results for the pack of solid beads in Fig. 8(b), where the propagators show no large stagnation peak, and the displacement distribution is considerably more compact than in the case of the porous beads, because most of the fluid contributes to flow. Surface relaxation has negligible effects on the measured mean displacements, while diffusion rounds the shape of the propagator as Δ is increased from 42 to 502 ms. This is due to diffusive coupling of stagnation zones to the flow field. The shape and width of the flow portion of the propagator are determined by mechanical mixing and are characteristic of the random pack of monodisperse spheres.

V. SIMULATION

In order to compare our results with a simple quantitative model we carry out diffusion-dispersion-relaxation simulations for Poiseuille flow in a cylindrical pipe with a leaky wall, behind which there is a reservoir of stagnant fluid coupled diffusively to the flow field, in the presence of surface relaxation. This is illustrated in Fig. 9. By design, the model will not capture the effects of mechanical mixing in our experiment, but it can simulate the evolution of the stagnation peak and illustrate the effects of (tunable) surface relaxation on propagators similar to those measured in the bead pack. The following relevant parameters for the pipe model are chosen to match our experiment. First, half the fluid is stagnant and the other half is flowing in the pipe. Second, the stagnant fluid is free to diffuse and its signal relaxes with a surface relaxation rate $(T_s)^{-1}=(395\ \text{ms})^{-1}$, producing a

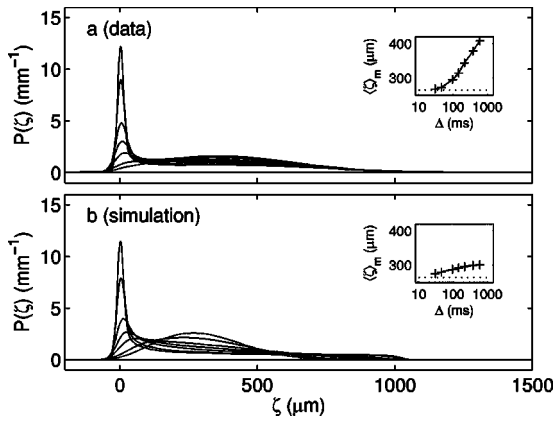

FIG. 10. (a) Propagators obtained for $\langle\zeta\rangle_0=265$ μm over times $\Delta=30$, 46, 96, 146, 213, 380, 600 ms, identified by decreasing height of the stagnation peak as Δ becomes larger. Inset shows the nominal mean displacement (dotted line) and the measured mean displacements (+) as a function of Δ. (b) Simulation results and plots for the equivalent pipe model described in the text.

NMR signal for the entire system with relaxation rate $(T_1)^{-1}\approx(790\ \text{ms})^{-1}$. Third, the pipe radius is chosen to have the same hydraulic radius r_h, defined as the flow cross-sectional area divided by the wetted perimeter, as a random pack of solid monodisperse spheres with radius $r_s=75$ μm and porosity $\phi=0.37$. For the random pack $r_h=(r_s/3)\times[\phi/(1-\phi)]\approx r_s/5$ and the equivalent pipe radius is therefore $r_p=(2/5)\times r_s=30$ μm. Fourth, molecules in the Poiseuille flow field diffuse freely in and across streamlines, with a semireflecting boundary condition ($\alpha=0.5$) at the wall. Here α is the probability that a molecule hitting the wall will make it through to the other side. Finally, the mean displacements and times simulated are the same as in the experiments, and the diffusion coefficient of water is used. Our model is reductive and simple, at the cost of some oversimplifications. We are assuming free diffusion and instantaneous equilibration in the stagnant zones, ignoring the fact that diffusion is actually restricted within the porous beads, and that spins located initially deep inside a porous bead may never diffuse out and into the flow. Also, as mentioned above, the pipe model produces no mechanical mixing.

We first compare modeling results with data in Fig. 10, for $\langle\zeta\rangle_0$ of 265 μm. The insets show $\langle\zeta\rangle_m$ as a function of Δ, indicating the degree to which surface relaxation has removed "slow" molecules from the measurement. Upon first inspection the similarities between data (a) and simulation (b) are rather good, with the stagnant peaks in model and experiment having similar amplitudes, widths, and time dependence. This suggests that our parametrization of the diffusive coupling and relaxation of stagnation zones is indeed reasonable. Simulated and experimental propagators differ in the appearance of the displacement spectrum associated with the flowing fluid between the spheres or in the pipe, with remnants of the rectangular displacement distribution characterizing Poiseuille flow in a pipe still recognizable in the simulation for the smallest choice of Δ. Diffusion across streamlines turns this into an approximately Gaussian shape by the time $\Delta=600$ ms. By contrast, the experimental data

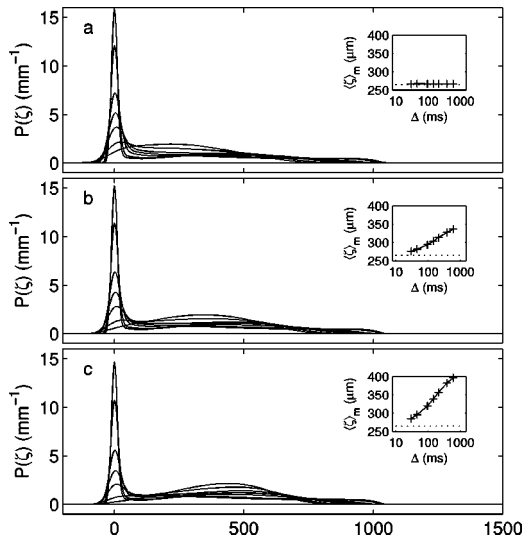

FIG. 11. Simulations illustrating the effect of surface relaxation on the shape of the propagators; mean displacements $\langle\zeta\rangle_0=265$ μm. The transmission coefficient for diffusive flux through the permeable wall of the pipe is set to $\alpha=0.1$. The surface relaxation time in the stagnation zone is adjusted to (a) $T_s=\infty$, (b) $T_s=395$ ms, and (c) $T_s=200$ ms. Evolution times Δ are as in the experimental results of Fig. 4.

show a more extended displacement spectrum, consistent with a distribution of pore diameters and mean flow velocities. The displacement distribution of the sample is less narrowed by diffusion than that of the pipe, again consistent with a distribution of mean pore velocities for the pores in the sample; the pores are separated by pore walls or distances larger than a diffusion length. The insets show that surface relaxation raises the measured mean displacement for growing evolution times Δ, to $\langle\zeta\rangle_m=400$ μm in the experiment and to $\langle\zeta\rangle_m=301$ μm in the simulation. The comparatively smaller enhancement of $\langle\zeta\rangle_m$ is probably due to the instantaneous equilibration of the stagnating fluid in the model, which tends to diminish displacement-relaxation correlations, and to the relative compactness of the model propagators. In these the overcount of displaced spins produces less excess mean displacement than it does in the comparatively stretched out propagators of the bead pack.

Finally, we show simulation results in Fig. 11 for three more sets of parameters, given in Table I. These illustrate the sensitivity of the simulation, and of the experiments, to surface relaxation. For all simulations in Fig. 11 we have set the transmission coefficient for diffusion through the porous

TABLE I. Results and parameters used for data and simulations.

Figure	T_s (ms)	$1-f$	α	$\langle\zeta\rangle_m$ [a]
10(a)				400
10(b)	395	0.50	0.5	301
11(a)	∞	0.50	0.1	265
11(b)	395	0.50	0.1	336
11(c)	200	0.50	0.1	396

[a] $\langle\zeta\rangle_0=265$ μm, $\Delta=600$ ms.

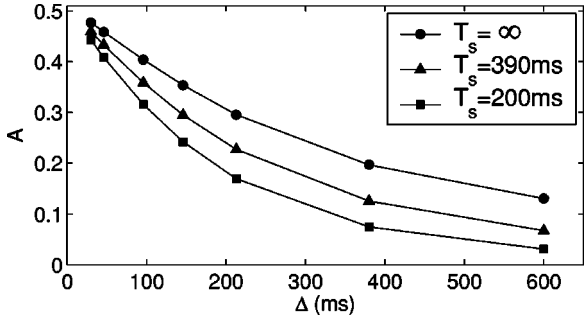

FIG. 12. Integrated area of the stagnation peak for the simulated propagators of Fig. 11. Integration limits are ± 60 μm. Half the fluid is located in stagnation zones, where the surface relaxation rate is set to T_s^{-1}.

pore wall to $\alpha=0.1$, compared to $\alpha=0.5$ for the semipermeable pore wall of the reference simulation in Fig. 10(b). The reduction of α produces a slightly more pronounced stagnation peak and increases the residence time for fluid in the stagnation zone in all panels. Figure 11(a) shows the propagators in the absence of surface relaxation, and panels (b) and (c) show what happens when the surface relaxation time T_s in the stagnation zone is set to 395 and 200 ms, respectively. As surface relaxation goes up, so does the long time measured mean displacement shown in the insets. The shape of that part of the propagators associated with the flow changes as surface relaxation is increased. Parts of the spectrum with small but finite displacements are suppressed, when compared with the true propagator obtained for no surface relaxation, because slow spins close to the pore wall have a relatively larger probability of having spent time in the stagnation zone, where relaxation could remove them from the measurement. As a result the displaced part of the spectrum becomes more rounded and shifts toward larger displacements. It should be noted that this is an instance where relaxation effects mimic the signature of an approach toward asymptotic dispersion, where one expects to see a rounded and ultimately Gaussian distribution of displacements about a mean displacement. The stagnation peak evolves by both diffusion and relaxation, quantified in Fig. 12 showing the integrated the area under the stagnation peaks of the simulated propagators as a function of Δ. In the absence of relaxation the stagnation peak initially contains about 48% of the fluid at $\Delta=30$ ms, which drops to 13% by the time $\Delta=600$ ms. When relaxation is turned on the short time amplitude of the stagnation peak drops by only a few percent, but for larger Δ the relaxation induced losses are much more significant, up to about 75%.

Our simulations show that even a crude model for dispersion in the presence of stagnant fluid can reproduce the stagnation features of propagators measured in our PFG experiments, when reasonable input parameters are chosen. They also show that surface relaxation gives rise to non-negligible distortions of propagators, particularly when the experimental time scale Δ is not small when compared to the shortest relaxation time scales, and that the comparison of nominal mean displacements with measured mean displacements provides a useful indicator for the presence of such distortions.

VI. CONCLUSION

PFG NMR measurements of displacement distributions provide a powerful tool for studying the geometry of porous media and fluid transport through them. As measurements are extended from the study of flow through magnetically clean laboratory systems, say packs of polystyrene spheres, to somewhat less ideal systems with non-negligible surface relaxation, internal field inhomogeneities, and complex pore spaces, the experimental results are distorted by NMR artifacts which can easily be mistaken for dispersion physics. In this work we have taken a controlled step toward measurements in such nonideal systems by performing PFG NMR propagator measurements on Stokes flow of water through a porous pack of glass beads. We optimized our sampling of q space to produce propagators with sufficient quality and resolution for detailed quantitative study of diffusion, dispersion, and NMR relaxation effects in the measurement. The measurements were performed as a function of space (mean displacement) and time separately, in order to keep track of the different physical mechanisms affecting our results. Surface relaxation processes and susceptibility induced variations of the internal fields affect nearly all PFG NMR measurements on flow through porous media, and we have demonstrated how these effects can be quantified and delineated. In the presence of surface relaxation we measure a lower bound on the number of spins diffusing out of stagnation zones and into the flow. Numerical simulations compare well with the experimental results, and furthermore show that, in order to minimize the distorting effects of surface relaxation on the measurement, the measurement time scale must be shorter than the shortest significant relaxation time scales.

ACKNOWLEDGMENT

J.G.S. acknowledges the support of the Norwegian Research Council. U.M.S. thanks Martin Hürlimann for useful discussions and suggestions regarding the manuscript.

[1] G.I. Taylor, Proc. R. Soc. London, Ser. A **219**, 186 (1953).
[2] G.I. Taylor, Proc. R. Soc. London, Ser. A **225**, 473 (1954).
[3] P.G. Saffman, J. Fluid Mech. **6**, 321 (1959).
[4] P.G. Saffman, J. Fluid Mech. **6**, 194 (1960).
[5] P.-G. de Gennes, J. Fluid Mech. **136**, 189 (1983).
[6] E.O. Stejskal and J.E. Tanner, J. Chem. Phys. **42**, 288 (1965).
[7] P.P. Mitra, P.N. Sen, L.M. Schwartz, and P. Le Doussal, Phys. Rev. Lett., **68**, 3555 (1992).
[8] J. Kärger and W. Henk, J. Magn. Reson. (1969-1992) **51**, 1 (1983).
[9] E. Charlaix, J.P. Hulin, and T.J. Plona, Phys. Fluids **30**, 1690 (1987).

[10] J.-P. Hulin and D. Salin, *Experimental Methods in Physical Sciences 35* (Academic Press, New York, 1999).
[11] L. Lebon, L. Oger, J. Leblond, J.-P. Hulin, N.S. Martys, and L.M. Schwartz, Phys. Fluids, **8**, 293 (1996).
[12] J.D. Seymour and P.T. Callaghan, J. Magn. Reson., Ser. A **122**, 90 (1996).
[13] J.J. Tessier, K.J. Packer, F.-F. Thovert, and P.M. Adler, AIChE J. **43**, 1653 (1997).
[14] B. Manz, P. Alexander, and L.F. Gladden, Phys. Fluids **11**, 259 (1999).
[15] G. A. Barrall, Ph.D. thesis, University of California, Berkeley, 1995.
[16] D. Kandhai, D. Hlushkou, A.G. Hoekstra, P.M.A. Sloot, H. Van As, and U. Tallarek, Phys. Rev. Lett. **88**, 234501 (2002).
[17] U.M. Scheven and P.N. Sen, Phys. Rev. Lett. **89**, 254501 (2002).
[18] K.H. Coats and B.D. Smith, Soc. Pet. Eng. J., p. 73 (March, 1964) (available at www.spe.org as Report No. SPE-674).
[19] L. Lebon and J. Leblond, J. Magn. Reson. **159**, 13 (2002).
[20] CPG03000A supplied by CPG Inc.
[21] R.M. Cotts, M.J.R. Hoch, T. Sun, and J.T. Markert, J. Magn. Reson. (1969-1992) **83**, 252 (1989).
[22] Y. Song, Phys. Rev. Lett. **85**, 3878 (2000).
[23] M. Toda, R. Kubo, and N. Saito, *Statistical Physics II*, 2nd ed. (Springer-Verlag, Berlin, 1991).